Antiproton-Proton Annihilation into Charged Pion and Kaon Pairs from 0.7 to 2.4 GeV/c*

H. Nicholson,† B. C. Barish, J. Pine, A. V. Tollestrup, and J. K. Yoh
California Institute of Technology, Pasadena, California 91109

C. Delorme,‡ F. Lobkowicz, A. C. Melissinos, and Y. Nagashima
University of Rochester, Rochester, New York 14627

A. S. Carroll and R. H. Phillips
Brookhaven National Laboratory, Upton, New York 11973

(Received 1 June 1972)

A counter-spark-chamber experiment has been performed to measure the annihilation reactions $\bar{p}p \to \pi^+\pi^-$ and $\bar{p}p \to K^+K^-$ in the energy region 0.7–2.4 GeV/c. The angular region covered in the experiment was $0.65 \leq |\cos\theta_{\text{c.m.}}| \leq 1.0$. The data were taken in order to study heavy bosons (mass greater than two nucleons) that might couple to the $\bar{p}p$ system. Our data have been combined with data from a previous BNL-Caltech experiment to give complete folded angular distributions and total cross sections for these reactions at 12 incident momenta. The folded two-pion annihilation data have been fitted by a simple Breit-Wigner resonance model in order to explore possible resonance behavior. The extreme-angle data have been interpreted in terms of particle exchanges, and through crossing symmetry comparisons are made with backward πp and Kp scattering.

I. INTRODUCTION

A partially separated antiproton beam at Brookhaven National Laboratory's Alternate Gradient Synchrotron (AGS) has been used in an experiment to measure the folded[1] cross sections for the reactions

$$\bar{p}+p \to \pi^+ + \pi^-, \tag{1}$$

$$\bar{p}+p \to K^+ + K^- \tag{2}$$

in the angular region $0.65 < |\cos\theta_{\text{c.m.}}| < 1.0$ at 14 momenta between 0.7 and 2.4 GeV/c. These data were taken simultaneously with data which measured backward elastic scattering of antiprotons. The $\pi\pi$ and KK cross sections, combined with those of Fong *et al.*[2] for $|\cos\theta_{\text{c.m.}}| < 0.70$, give complete folded angular distributions for 12 momenta in this momentum range. In addition, in the angular region $0.90 < |\cos\theta_{\text{c.m.}}| < 1.0$ the sign of the charge of the forward-going meson was determined.

Differential and total cross-section measurements of reactions (1) and (2) are of great interest since they provide a way to search for very heavy boson resonances (mass greater than two nucleons). The Feynman diagrams which show possible direct-channel-resonance quantum numbers for reactions (1) and (2) are given in Fig. 1. Groups at Brookhaven,[3,4] CERN,[5] and Michigan[6] have reported various $B=0$ structures with masses between 1990 and 2570 GeV which could be due to boson resonances.

Since the antinucleon-nucleon ($\bar{N}N$) system is an isospin-0 or -1 system and the parity of the antimeson-meson ($\bar{M}M$) system is $(-1)^J$, where J is the total spin, s-channel resonances in the annihilation reaction $\bar{N}N \to \bar{M}M$ must have $I=0$ with even J or $I=1$ with odd J. Hence, any resonance coupled to the $\bar{p}p \to \bar{M}M$ system whose spin J can be determined from a study of the angular distribution will have its isospin and parity quantum numbers determined as well.

In addition to providing a means to search for heavy-meson resonances, cross-section measurements of the backward cross sections[7] for the reactions

$$\pi^\pm + p \to p + \pi, \tag{3}$$

$$K^\pm + p \to p + K \tag{4}$$

can be used to test theoretical models relating reactions (1) to (3) and (2) to (4) (see Ref. 8) at extreme angles. Figure 2 shows how the amplitude for the backward elastic scattering reaction $MN \to MN$ can be related via crossing symmetry and the assumption of dominant u-channel exchanges to the amplitude for the annihilation reaction $\bar{N}N \to \bar{M}M$. With the usual definition of s, t, and u, the energy variable in the backward elastic scattering reaction, s, becomes t in the annihilation reaction, while the u variable remains the same. At energies where a single u-channel or fermion Regge-pole exchange dominates the cross section, u-channel amplitudes in the backward elastic scattering reaction can be used to obtain the u-channel

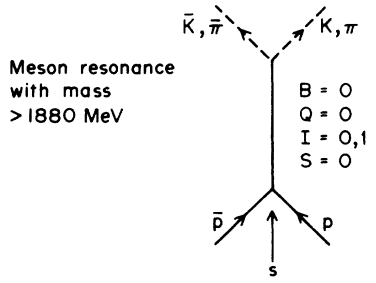

FIG. 1. s-channel resonance formation for the reactions $\bar{p}p \to \pi\pi$ and $\bar{p}p \to KK$.

amplitudes in the annihilation reaction by making the replacement $s \to u$, or $z_u \to -z_u$ where $z_u = \cos\theta_u$.

The reactions $\bar{p}p \to k^+k^-$ and $k^-p \to pk^-$ are of special interest since an exotic $S = +1$ baryon, the Z^{*++}, is required if the amplitudes are dominated by a single u-channel exchange. Such a baryon cannot be formed in the quark model by three quarks.

Previously published $\bar{p}p \to \bar{M}M$ data are scanty because of the difficulty in obtaining high-flux $\bar{p}$ beams and because two-meson final-state annihilation cross sections are small ($\sigma^{\text{total}}_{\bar{p}p \to \pi\pi} \sim 200$ μb) relative to other processes which can occur ($\sigma^{\text{total}}_{\bar{p}p} \sim 100$ mb). Bubble-chamber experiments at Berkeley[9] and Michigan[10] have measured differential and total cross sections between 1.6 and 2.2 GeV/c for reactions (1) and (2) with considerably poorer statistics than those given below.

At lower momenta our results are supplemented by the bubble-chamber data of Bizzarri *et al.*[11] Recently, a counter–spark-chamber experiment has measured the annihilation cross section at 5 GeV/c.[12] Also, the polarization for two-pion annihilation has been measured at 1.64 GeV/c.[13]

II. DESCRIPTION OF EXPERIMENT

A. The Beam

This experiment was performed in the short branch of the partially separated beam at the Brookhaven National Laboratory AGS. The $\bar{p}$ fluxes for this beam ranged between 500 $\bar{p}$'s at 0.68 GeV/c and 45 000 $\bar{p}$'s at 2.40 GeV/c, with each pulse lasting about 0.5 sec at a machine repetition rate of 25 pulses/min.

Antiprotons were selected by using both a liquid differential Čerenkov counter[14] and a time-of-flight system. For momenta of 1.0 GeV/c and greater, only the C counter was needed to reduce the pion contamination under the $\bar{p}$ peak to less than 5%. At 2 GeV/c, the efficiency of the C counter for antiprotons was measured to be better than 90%.[15] At low incident momenta (0.7–1.0 GeV/c) both a time-of-flight (TOF) system and the Čerenkov counter were needed to obtain sufficient rejection of pions. The difference in flight time between π's and $\bar{p}$'s

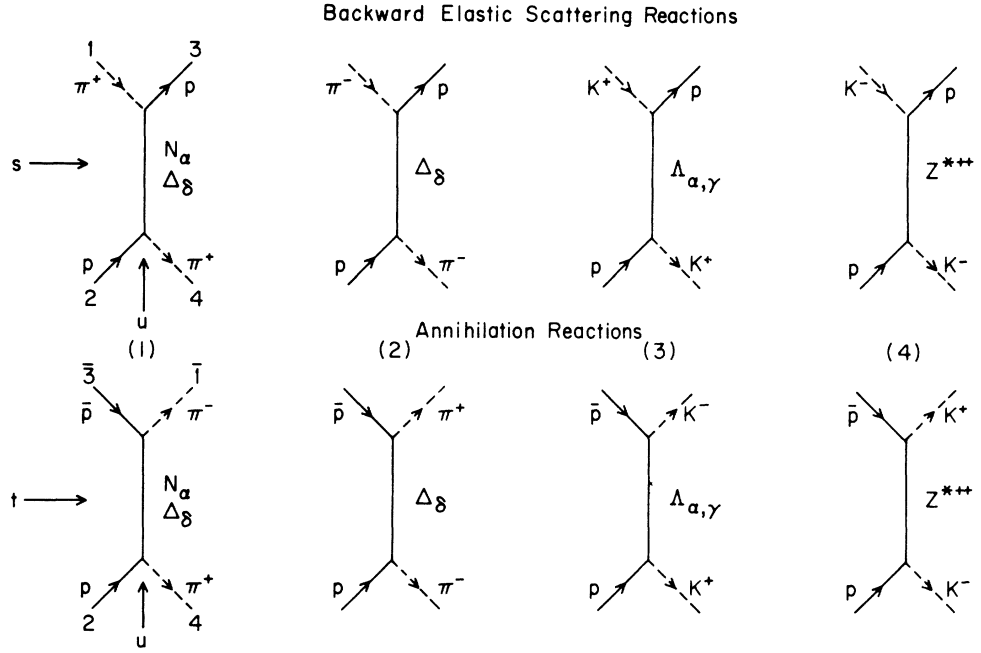

FIG. 2. Exchange diagrams for the four pairs of backward-scattering and annihilation reactions. Reaction 1 indicates how the top two arms of the diagram are interchanged to give the s and t channels. Some of the possible exchanged baryon trajectories are included.

traversing the 41 ft between the TOF counters at these momenta was ~4 nsec. The C counter (set to accept pions) was put in anticoincidence with the TOF system.

A beam particle was defined by three beam-defining scintillation counters arranged so that a threefold coincidence (defined as $S = S_1S_2S_3$) in them required the incident particle to traverse the hydrogen target. A pile-up gate was used to help prevent multiple beam tracks in the spark chambers. This gate typically reduced the amount of usable beam by 10–30%.

B. Experimental Layout

The experimental layout is shown in Fig. 3. It is similar to the layout used in the Rochester-BNL pion and kaon backward-scattering experiments[16] except for the longer liquid-H_2 target ($14\frac{5}{8}$ in. long) and the addition of several scintillation counters.

A two-particle final-state annihilation is characterized by an incident beam particle, a backward-scattered particle, and a forward-going particle. In our experiment, when a beam antiproton (defined by the S and C counters) interacted in the target, scintillation-counter arrays upstream of the target (B counters), downstream of the target and upstream of the magnet (P counters), and downstream of the magnet (Q and R counters) were used to determine this event topology and to trigger three sets of four wire spark chambers, one set in each region. In addition, anticounters (A counters) in the beam and surrounding the target were used in the event trigger to ensure that the beam particle disappeared and to reduce backgrounds from multiparticle final-state interactions. The counters surrounding the target had lead plates for converting γ rays from π^0 decay. A 4 ×4 matrix of beam hodoscope counters was used to select the correct beam track for events with multiple beam tracks in the upstream wire chambers.

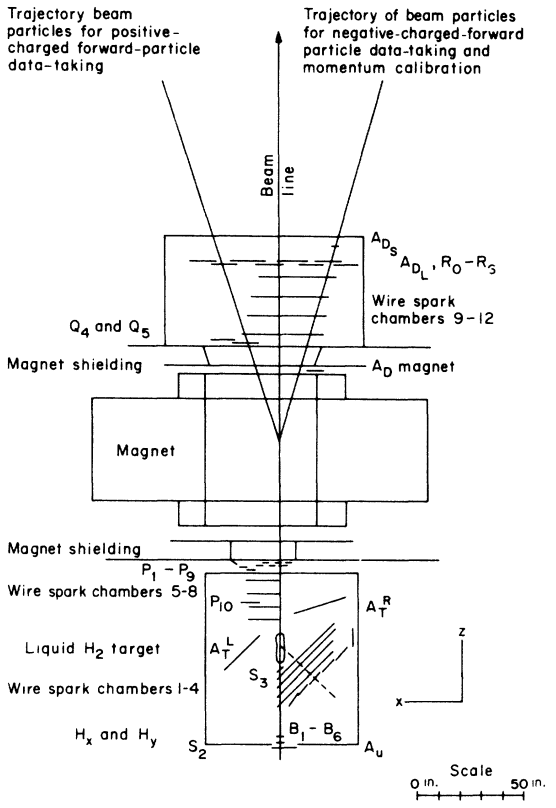

FIG. 3. Layout of the experimental apparatus.

The upstream wire spark chambers, positioned at a 45° angle with respect to the beam line, detected both beam and backward-scattered particles. The array of chambers between the target and the bending magnet were used to detect the forward-scattered particle, and the array of chambers downstream of the magnet in conjunction with the bending magnet formed a momentum spectrometer for forward-going particles. Spark positions in the chambers were digitized by a magnetostrictive readout system under the control of a PDP-8 computer. Events stored into the computer during the beam spill were written on magnetic tape between bursts.

The magnet used in this experiment was a 48D48 with an 18-in. vertical aperture. In addition to determining the sign of the charge for small-angle annihilation reactions (reactions whose forward-scattered particle formed laboratory angles of less than 15° in the horizontal plane and ±5° in the vertical plane), accurate central-field measurements using a nuclear magnetic-resonance probe and an effective-field-length equation derived from previous detailed field measurements made it possible to calculate the momenta of beam and small-angle event particles traversing the downstream wire spark chambers to 0.3%.[17]

C. The Spark-Chamber Trigger

Only those events characterized by a disappearing beam antiproton and no signal in target anticounters could produce wire-spark-chamber triggers. The triggers were either (a) wide-angle triggers, or (b) downstream triggers.

Events characterized by coincidences between wide-angle B counters (B_3–B_6) and a wide-angle P counter (P_6–P_{10}) were wide-angle trigger events. The sign of the charge of the reaction particles for these events was not determined.

Events characterized by threefold coincidences between a small-angle B counter (B_1–B_5), a small-

angle P counter (P_1–P_6), and either a Q or an R counter were downstream trigger events. Since the forward-going particle traversed the bending magnet, the sign of its charge was determined. Those downstream trigger events in which the forward-going particle formed an angle of less than 5° with the beam line and traversed the downstream wire chambers had the momentum as well as the sign of the charge of the forward particle determined.

By changing the direction of the magnetic field, the trigger was alternately set for negatively and positively charged forward-going particles. The beam trajectories for both magnet settings are shown in Fig. 3.

D. The Wire Spark Chambers

The wire spark chambers used in this experiment consisted of two planes of parallel coplanar wires 20/in. and 25 mil wide etched onto Mylar sheets 3 to 4 mil thick, spaced 0.25 in. apart and oriented so that the wires in each plane were at right angles to each other.[18] The fiducial wires at either extreme of the chamber's sensitive area were included on each wire plane and pulsed for every event. Twelve hydrogen thyroton pulsers provided the high voltage for each individual chamber. A magnetostrictive readout system[19] and four 10-MHz scalers (giving a capacity of 4 sparks/coordinate) were used to digitize spark coordinates. The precision of the system was essentially that of the scaler least count (±0.52 mm). The 24 coordinates on the 12 chambers were connected in series and read out sequentially to the digitizer and into a PDP-8 computer.

III. ANALYSIS OF DATA

A. Reconstruction

The spark coordinate and counter bit information written on magnetic tape for each event was converted into proton-antiproton annihilation cross sections by means of an event-reconstruction computer program, which was run on the Brookhaven CDC-6600 computer. Event candidates obtained from the reconstruction procedure were further analyzed by means of a separate program.

Track-finding by the reconstruction program was performed separately in each array of four wire chambers. All possible two-spark tracks for a given coordinate between the furthest upstream chamber of an array (chamber 1) and the chamber with the minimum number of sparks for that coordinate (except chamber 2) were found and extrapolated to the other chambers in the array. When sparks could be found in both of the other chambers within 7.5 mm from the extrapolation, a line was fitted to the four sparks using a least-squares procedure. After all four spark tracks had been obtained in a given region, the spark coordinates used to form them were removed from consideration and a search was made for all three spark tracks in that region.

Once all the tracks had been found, they were identified in the following manner. In the horizontal projection of the chambers upstream of the target (region 1) the track at an angle of less than 50 mrad was classified as a beam track. Note that there should be at least two tracks in this region, corresponding to the beam track and the backward-scattered particle. This beam region eliminated the need for rotating some of the upstream wire chambers to remove track ambiguities. In the vertical projections where there was more than one track, the track corresponding to the correct beam hodoscope counter was selected as the beam track. Tracks in the chamber arrays between the target and the magnet (region 2) were called forward tracks and those in the chambers downstream of the magnet (region 3) were called magnet tracks.

For the widest-angle events the forward-going particle was only required to traverse the two wire spark chambers downstream of and nearest to the target. For these events the track was defined by a least-squares fit to the interaction vertex in the target and the sparks in the two chambers.

Frequently (~20% of the time) extra tracks (more than two tracks in region 1 and/or more than one in regions 2 and 3) were found for a particular event. These extraneous tracks were removed in the analysis by keeping only beam tracks due to particles which interacted in the target and passed through the appropriate beam hodoscope counter. Then if any ambiguity remained we chose the pair of tracks in region 1 and the track in region 2 which formed the best vertex within the fiducial target volume. Extra tracks were never a problem in region 3.

The final reconstructed event always consisted of a beam track, a backward scattered track, and a forward scattered track, and sometimes included a magnet track. Events whose tracks formed a vertex with a copunctuality[20] limit of less than 1 cm inside the target volume, which were coplanar to within ±50 mrad, and which satisfied broad kinematical constraints were then recorded on magnetic tape.

B. Event Determination

The events having approximately the topology and kinematics for $\bar{p}p \to \pi^+\pi^-$ or K^+K^- were studied

further by calculating the final-state particle squared masses assuming equal-mass two-particle states. The final-state particle squared masses in the forward direction were calculated from the forward-scattered particle momenta and the scattering angles of the backward-scattered particles. The final-state particle squared masses for the wider-angle scattering events were calculated from the forward and backward scattering angles of the final-state particles, alone. These two methods of calculation enable the two-pion and two-kaon annihilations to be adequately separated from each other for all angles, from 0° to the widest-angle scattering which could be measured in this experiment.

Events whose beam and backward- and forward-scattered particle tracks were coplanar to within 15 mrad were considered two-body annihilation events, and those events whose tracks were coplanar to within 30 mrad but greater than 15 mrad were used to estimate the multiparticle background. This background was subtracted bin by bin from the annihilation-event candidates in the cross-section calculation. The acceptable final-state particle squared-mass ranges for two-pion and two-kaon annihilations were chosen to be -0.14 to $+0.16$ GeV^2 and $+0.16$ to $+0.35$ GeV^2, respectively.

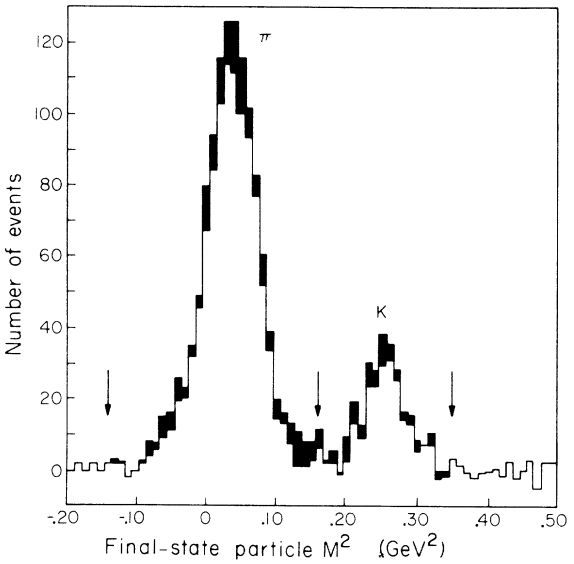

FIG. 4. Distribution of squared masses of final-state particles assuming equal-mass two-particle final states. Squared masses were calculated from the incident $\bar{p}$ momentum and the forward and backward scattering angles. The above data were obtained at 0.99-GeV/c incident $\bar{p}$ momentum with the trigger set for a negative forward-going particle. The shaded events are the wrong-charge tracks, which have been removed from the sample.

The experimental acceptance was such that forward-going particles near the beam line with charge signs opposite to the trigger setting could traverse the magnet and satisfy fast-logic trigger conditions. These wrong-sign–particle events were removed from the event sample using scintillation-counter bit information downstream of the magnet and wire-spark-chamber trajectory information upstream of the magnet.

Event candidates were further required to have tracks whose vertex fell within the target volume and which were copunctual[20] to within 0.5 cm. The accurate vertex definition of $\lesssim 0.5$ cm eliminated the need for empty-target subtraction. Wire-chamber fiducial cuts were made to ensure that a backward-going final-state particle traversed a trigger counter and that a forward-going final-state particle had negligible probability of hitting a magnet pole face. All topological cuts were identical with those used in a Monte Carlo calculation of the experimental detection solid angles.

Figure 4 gives a plot of final-state particle squared masses for event candidates with the off-

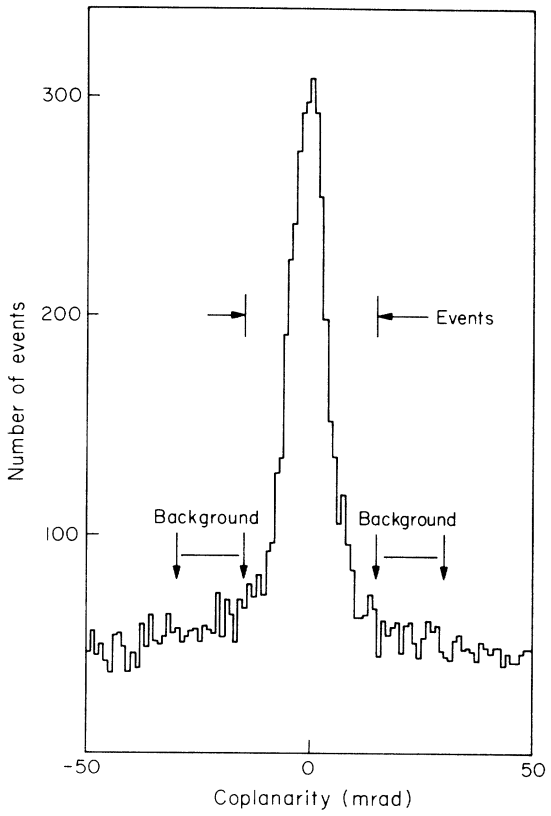

FIG. 5. Distribution of coplanarity at 0.99-GeV/c incident $\bar{p}$ momentum with the trigger set for a negative forward-going particle. Events were required to have beam, backward-scattered, and forward-scattered tracks coplanar to within ±15 mrad.

coplanar background subtracted out at 0.99 GeV/c for a negative particle going forward. The shaded events are the wrong-charge tracks which have been removed from the sample. The coplanarity distribution before background subtraction for the same events is given in Fig. 5.

C. Cross-Section Calculation

The differential cross sections and their statistical errors were calculated from the formulas

$$\frac{\Delta\sigma_{\pi,K}}{\Delta\Omega}(\theta)=\frac{\Delta N_{\pi,K}(\theta)}{\Delta\Omega}\left(\frac{1}{N_0 nL}\right), \tag{5}$$

$$\epsilon_s=\frac{\Delta\sigma}{\Delta\Omega}(\theta)\left[\frac{(N_T+N_B)^{1/2}}{N_T-N_B}\right], \tag{6}$$

where N_0 is the number of antiprotons incident on the target, n is the number of scattering protons per unit volume in the target, $\Delta N_{\pi,K}(\theta)$ is the number of pions and kaons scattered at center-of-mass angle θ, L is the length of the target, and N_B, N_T are respectively the raw number of background events and the total number of events used in the cross-section calculation.

The effective solid angle $\Delta\Omega$ for $\cos\theta_{c.m.}$ bins of 0.02 was calculated using a Monte Carlo method. This calculation was done separately for those events in which the forward-going particle traversed the magnet and the wire spark chambers downstream of the magnet, those events in which the forward-going particle traversed the magnet but not the wire spark chambers downstream of the magnet, and those events in which the forward-going particle only went through the chambers upstream of the magnet. 10 000 trials for each charge-sign trigger at each momentum gave statistical uncertainties in the solid angle of 10%.

In order to correct for experimental and event-reconstruction inefficiencies, studies were made to determine the magnitudes of the systematic errors associated with this experiment. Corrections to the normalization were made to account for scintillation-counter inefficiencies [(4 ± 1.2)%], wire-chamber inefficiencies (5–10%), event-reconstruction inefficiencies [(7.0 ± 1.1)%], events lost to accidentals in the trigger veto counters [(1.3 ± 0.3)%], a flux correction for the absorption of beam in the hydrogen target [(~10 ± 1.5)%], and event losses due to final-state particle nuclear interactions in the experimental apparatus [(~4 ± 2)%]. Angle-dependent corrections other than those included in the beam absorption and nuclear interaction of final-state particles include the inefficiency in the reconstruction procedure for events whose forward final-state particle traversed the magnet [(3.5 ± 3.5)%] and for wide-angle events [(1 ± 1)% for $0.7 \leq |\cos\theta_{c.m.}| < 0.8$ and (2.5 ± 2.5)% for 0.6

TABLE I. Extreme-angle pion cross sections $d\sigma/d\Omega$ (μb/sr).

$\cos\theta_{c.m.}$	Momentum (GeV/c) 0.700	0.810	0.870	0.990	1.120	1.340	1.450	1.590	1.710	1.815	2.000	2.160	2.260	2.400
0.99	156.3 ± 52.1		70.7 ± 12.6	54.1 ± 6.7	31.5 ± 5.1	31.6 ± 5.5	34.3 ± 5.1	19.1 ± 3.8	18.2 ± 4.2	17.4 ± 2.5	19.2 ± 3.5	17.6 ± 2.4	13.3 ± 3.2	9.9 ± 2.3
−0.99	123.6 ± 31.9	81.8 ± 27.3	96.9 ± 15.9	97.9 ± 9.9	87.4 ± 15.2	27.8 ± 3.9	25.0 ± 5.0	15.7 ± 3.0	16.7 ± 3.4	9.1 ± 1.9	3.9 ± 1.6	5.4 ± 1.6		2.8 ± 1.2
0.96	75.4 ± 29.5		85.8 ± 11.5	70.5 ± 6.6	40.5 ± 3.4	34.7 ± 6.7	19.8 ± 4.7	21.3 ± 3.5	15.0 ± 4.7	12.3 ± 1.4	10.8 ± 3.5	15.8 ± 1.5	9.2 ± 2.9	3.9 ± 1.5
−0.96	153.6 ± 28.4	101.9 ± 27.1	120.3 ± 16.1	94.6 ± 8.3	75.2 ± 12.8	23.2 ± 4.0	23.6 ± 5.6	8.2 ± 2.0	4.2 ± 3.0	6.6 ± 1.0	5.4 ± 1.7	6.8 ± 1.8		3.4 ± 1.4
0.92			58.5 ± 15.0	86.5 ± 11.3	34.1 ± 4.4	35.7 ± 6.4	8.8 ± 3.4	7.8 ± 2.5	4.2 ± 6.0	7.0 ± 1.3	10.0 ± 5.8	13.9 ± 3.4	16.7 ± 5.9	5.0 ± 3.8
−0.92			69.2 ± 17.5	94.4 ± 12.7	59.3 ± 15.0	20.7 ± 4.1	12.3 ± 4.5	4.0 ± 1.6	9.6 ± 3.8	2.7 ± 1.4	3.1 ± 2.7	1.7 ± 1.7		6.2 ± 2.6
0.88						45.6 ± 12.2	7.5 ± 6.6		5.7 ± 4.1	4.4 ± 1.9	0.0	4.1 ± 1.6		2.2 ± 2.9
−0.88						16.5 ± 5.0	26.1 ± 8.0		4.9 ± 2.8	0.0	...	0.0		3.5 ± 3.9
										...	3.4 ± 2.6	...		
0.84										3.1 ± 3.9	0.0	0.0		
−0.84											...	...		
										3.5 ± 2.0	3.1 ± 3.1	3.4 ± 3.4		

TABLE II. Extreme-angle kaon cross sections $d\sigma/d\Omega$ (μb/sr).

	Momentum (GeV/c)													
$\cos\theta_{c.m.}$	0.700	0.810	0.870	0.990	1.120	1.340	1.450	1.590	1.710	1.815	2.000	2.160	2.260	2.400
0.99	10.9 ± 10.9		19.5 ± 7.7	14.6 ± 4.4	12.0 ± 3.7	7.1 ± 3.3	12.7 ± 5.5	12.0 ± 3.2	7.7 ± 3.7	8.8 ± 2.0	10.2 ± 2.9	7.4 ± 1.9	4.9 ± 2.6	6.5 ± 2.1
−0.99	63.0 ± 23.1	30.1 ± 22.5	16.3 ± 10.8	33.9 ± 6.6	23.6 ± 11.0	13.5 ± 3.8	4.1 ± 2.9	4.0 ± 2.0	0.0	1.2 ± 0.9	0.6 ± 1.0	1.1 ± 1.1		0.0
									•••					•••
0.97	32.3 ± 27.6			18.6 ± 6.6										
−0.97	50.2 ± 27.6			26.4 ± 7.7										
0.96					16.6 ± 3.3					9.9 ± 1.4	2.6 ± 1.7		5.5 ± 2.0	4.2 ± 1.5
−0.96		33.9 ± 17.9			22.9 ± 12.0					1.0 ± 0.6	2.0 ± 1.0			0.7 ± 0.7
0.95						7.1 ± 3.3	9.7 ± 3.2		9.4 ± 3.3			7.5 ± 1.1		
−0.95						6.3 ± 2.1	5.5 ± 2.4		1.5 ± 3.3			0.0		
												•••		
0.94			17.1 ± 5.0					9.1 ± 1.8		8.1 ± 0.8				
−0.94			11.0 ± 4.5					2.4 ± 1.2		1.8 ± 0.7				
0.92				17.4 ± 3.9	13.5 ± 3.6						6.5 ± 5.6		2.4 ± 2.4	3.2 ± 3.9
−0.92				21.1 ± 4.9	20.9 ± 12.0						0.0			2.0 ± 2.0
											•••			
0.89												6.1 ± 1.6		10.3 ± 10.3
−0.89												0.0		2.1 ± 1.6
												•••		
0.88											6.7 ± 8.1			
−0.88											0.0			
											•••			

TABLE III. Folded pion cross sections $d\sigma/d\Omega(\theta) + d\sigma/d\Omega(\pi - \theta)$ (μb/sr).

	Momentum (GeV/c)													
$\cos\theta_{c.m.}$	0.70	0.81	0.87	0.99	1.120	1.340	1.450	1.590	1.710	1.815	2.000	2.160	2.260	2.400
0.91	126.5 ± 26.6	157.7 ± 27.4		132.7 ± 8.0										
0.89							34.5 ± 3.9		7.2 ± 2.9				6.8 ± 3.7	
0.87					68.5 ± 3.3			7.3 ± 2.4						
0.85	134.9 ± 24.4	144.3 ± 23.5		122.2 ± 6.7						6.5 ± 1.1				
0.83						32.0 ± 2.9	29.8 ± 3.1		8.5 ± 2.9		5.9 ± 2.4		9.5 ± 3.6	4.8 ± 2.2
0.82			117.5 ± 8.1											
0.81								12.4 ± 2.1						
0.80					56.9 ± 2.4							5.6 ± 0.8		
0.79		68.6 ± 15.8		97.1 ± 6.3						11.0 ± 0.9				
0.77	107.3 ± 17.7					28.4 ± 3.1			12.9 ± 2.8		8.0 ± 2.1		4.3 ± 2.9	5.6 ± 3.2
0.76							31.0 ± 3.4							
0.75			56.0 ± 10.4					21.8 ± 2.9						
0.73		135.1 ± 25.9								14.6 ± 1.2				
0.72				75.8 ± 5.7	42.1 ± 3.2							5.8 ± 1.8		
0.71						33.6 ± 5.3			18.2 ± 3.7		12.0 ± 2.8		7.8 ± 2.9	10.7 ± 4.5
0.69								27.7 ± 3.7						
0.68							33.9 ± 4.1							
0.67	74.0 ± 20.1	73.3 ± 26.3								15.3 ± 1.9				
0.65				53.1 ± 7.3					18.3 ± 4.3		14.2 ± 3.3	5.5 ± 4.8		
0.64					48.1 ± 5.5								11.2 ± 6.0	
0.63								21.6 ± 4.7						

TABLE IV. Folded kaon cross sections $d\sigma/d\Omega(\theta) + d\sigma/d\Omega(\pi - \theta)$ (μb/sr).

	Momentum (GeV/c)													
$\cos\theta_{c.m.}$	0.70	0.81	0.87	0.99	1.120	1.340	1.450	1.590	1.710	1.815	2.000	2.160	2.260	2.400
0.91		45.3 ± 14.9	18.5 ± 6.1	25.1 ± 4.3	16.5 ± 2.8									
0.90	121.9 ± 28.6													
0.87						7.9 ± 2.5				10.1 ± 0.7			5.6 ± 2.4	
0.85	68.3 ± 16.6	79.8 ± 28.2	32.1 ± 5.1	22.9 ± 3.6	10.1 ± 1.4						4.9 ± 2.2	7.3 ± 1.1		
0.83							7.7 ± 2.8		11.6 ± 2.8					
0.81						4.7 ± 1.7							5.3 ± 4.6	5.8 ± 2.7
0.80								7.3 ± 1.7						
0.79	58.7 ± 15.7	51.4 ± 21.0	29.5 ± 7.4	23.8 ± 4.2	11.1 ± 1.9									
0.77							9.9 ± 3.1		7.8 ± 3.1	8.1 ± 0.6				
0.75						8.2 ± 3.0					9.0 ± 2.0	6.8 ± 0.8	10.7 ± 4.2	
0.73		71.6 ± 22.9	22.3 ± 8.6	13.5 ± 4.4	9.3 ± 2.2			7.4 ± 2.1						
0.72	20.5 ± 8.8													
0.71							12.0 ± 3.6		10.6 ± 3.8					
0.69						9.8 ± 3.8							12.8 ± 9.0	
0.67		42.7 ± 17.5		17.6 ± 4.7						7.5 ± 0.9				
0.66											7.1 ± 2.6			
0.65							9.1 ± 3.5	11.9 ± 3.0	10.5 ± 3.3					
0.64	44.4 ± 25.8													
0.63													8.4 ± 4.2	
0.62				21.2 ± 6.9										

TABLE V. $\bar{p}p \to \pi\pi$ Legendre-expansion coefficients, in μb/sr.

Momentum (GeV/c)	$2\pi a_0$	a_2	a_4	a_6	a_8	a_{10}	χ^2	Prob.
0.700	358.4 ± 22.5	123.0 ± 12.6	76.1 ± 16.0				15.6	0.08
0.870	352.6 ± 12.5	103.6 ± 6.6	65.8 ± 7.3	−24.6 ± 8.1	−26.8 ± 10.6	−9.7 ± 8.9	8.6	0.38
0.990	342.1 ± 7.1	90.1 ± 3.3	50.4 ± 4.2	−35.8 ± 4.8	−9.8 ± 5.6	5.4 ± 5.3	25.7	0.002
1.120	243.6 ± 6.0	44.7 ± 3.4	41.7 ± 4.6	−7.7 ± 4.6	17.3 ± 4.6	0.4 ± 4.4	11.3	0.33
1.340	163.6 ± 4.9	20.0 ± 2.3	23.6 ± 2.8	−10.4 ± 2.9	9.3 ± 3.9	−5.5 ± 4.0	9.7	0.46
1.450	145.0 ± 3.9	15.4 ± 1.8	13.1 ± 2.5	−7.5 ± 2.7	17.4 ± 3.0	2.5 ± 3.0	20.4	0.04
1.590	98.5 ± 3.3	2.4 ± 1.3	7.3 ± 1.8	0.9 ± 2.0	22.3 ± 2.4	0.8 ± 2.6	20.7	0.04
1.710	82.8 ± 3.3	2.9 ± 1.5	4.3 ± 2.1	3.6 ± 2.2	19.8 ± 2.5	−1.7 ± 2.5	4.0	0.95
1.815	66.7 ± 2.0	2.5 ± 0.7	2.4 ± 1.0	2.2 ± 1.1	15.7 ± 1.4	−3.6 ± 1.5	14.3	0.22
2.000	59.7 ± 2.5	3.3 ± 1.1	2.1 ± 1.4	5.7 ± 1.6	9.1 ± 2.0	−5.4 ± 1.9	5.9	0.82
2.160	43.1 ± 1.6	5.4 ± 0.7	4.7 ± 0.9	7.5 ± 1.0	4.5 ± 1.3	−3.2 ± 1.2	22.7	0.01
2.400	28.0 ± 2.5	3.7 ± 1.1	0.4 ± 1.2	3.1 ± 1.5	1.3 ± 1.9	−1.0 ± 1.7	10.4	0.32

$\leq |\cos\theta_{\text{c.m.}}| < 0.7$]. Checks showed that systematic errors would not significantly affect the relative values of the angular distributions.

The cross sections calculated from the raw data were then averaged over a sufficient number of bins to give a reasonable statistical error. The final cross sections were calculated from these averaged cross sections and the normalization correction $N(\theta)$ from the equation

$$\left.\frac{d\sigma}{d\Omega}(\theta)\right|_{\text{final}} = \left.\frac{d\sigma}{d\Omega}(\theta)\right|_{\text{raw data}} [1 + N(\theta)]. \quad (7)$$

IV. RESULTS

Final cross-section results for this experiment are given in Tables I–IV, where $\cos\theta_{\text{c.m.}} = +1.00$ refers to a negatively charged forward-going meson. Tables V and VI give the coefficients a_l of Legendre-polynomial fits to the folded data of the form

$$\frac{d\sigma}{d\Omega}(\theta) + \frac{d\sigma}{d\Omega}(\pi - \theta) = \sum_{l=0}^{L} a_l P_l(\cos\theta), \quad l \text{ even} \quad (8)$$

since odd-l terms cannot contribute to the folded distributions. The total cross sections given in these tables have been obtained by integrating the fitted curve. Tables VII and VIII give, respectively, pion and kaon extreme-angle cross sections $d\sigma/d\Omega$ and $d\sigma/du$. All errors given in the tables are statistical. The over-all normalization uncertainty was 6%.

Figures 6 and 7 present the folded differential cross sections for the two-pion and two-kaon annihilations. The two-pion annihilation shows a more striking energy dependence. At the lowest momentum for this reaction there is a fairly simple distribution with peaks at $|\cos\theta_{\text{c.m.}}| = 0$ and 1.0. At 1.45 GeV/c a second dip begins to appear at $|\cos\theta_{\text{c.m.}}| \approx 0.85$, and then up to 2.0 GeV/c there are two very pronounced dips which change with energy. This double-dipped distribution is also seen in the energy-averaged data of Chapman *et al.*[21] Finally, at the highest momenta, the peak at $|\cos\theta_{\text{c.m.}}| = 0$ rapidly falls away.

The two-kaon annihilations also show energy-dependent changes, particularly in the vicinity of

TABLE VI. $\bar{p}p \to KK$ Legendre-expansion coefficients, in μb/sr.

Momentum (GeV/c)	$2\pi a_0$	a_2	a_4	a_6	a_8	a_{10}	χ^2	Prob.
0.700	158.2 ± 17.2	68.4 ± 9.4	32.4 ± 9.1	−24.0 ± 10.4	−34.1 ± 12.0	−15.1 ± 8.7	6.7	0.75
0.870	81.5 ± 5.9	16.6 ± 2.9	4.1 ± 4.0	−4.9 ± 5.0	−3.8 ± 4.9	2.9 ± 4.4	14.7	0.10
0.990	92.4 ± 4.3	20.1 ± 2.0	9.2 ± 2.7	5.7 ± 3.1	2.0 ± 3.3	1.9	7.2	0.84
1.120	63.0 ± 3.9	9.5 ± 2.2	13.0 ± 3.2	6.9 ± 3.3	4.6 ± 3.1	1.9 ± 2.8	7.4	0.69
1.340	40.4 ± 3.1	3.5 ± 1.5	4.8 ± 1.9	2.6 ± 2.0	5.0 ± 2.5	3.5 ± 2.6	7.6	0.58
1.450	44.4 ± 2.9	7.1 ± 1.5	5.6 ± 1.9	−1.7 ± 2.3	−2.1 ± 2.3	−1.1 ± 2.0	13.4	0.20
1.590	37.3 ± 2.6	6.0 ± 1.1	3.9 ± 1.4	−1.4 ± 1.7	1.2 ± 2.1	1.6 ± 1.9	11.0	0.20
1.710	38.2 ± 3.0	6.9 ± 1.4	1.3 ± 1.7	−5.8 ± 1.8	−2.0 ± 2.2	−0.5 ± 2.1	8.3	0.60
1.815	32.3 ± 1.3	5.9 ± 0.5	2.0 ± 0.7	−4.2 ± 0.8	1.8 ± 1.0	−0.4 ± 1.0	8.1	0.42
2.000	23.0 ± 2.3	2.7 ± 1.0	1.5 ± 1.1	−1.8 ± 1.5	2.6 ± 1.8	1.1 ± 1.5	13.2	0.16
2.160	21.1 ± 1.2	4.8 ± 0.5	2.1 ± 0.7	−3.2 ± 0.9	−0.1 ± 1.0	2.3 ± 0.9	10.4	0.17
2.400	13.2 ± 2.5	4.2 ± 1.0	2.0 ± 1.0	−2.0 ± 1.5	−1.3 ± 1.4	−0.8 ± 1.3	9.4	0.23

TABLE VII. Pion extreme-angle differential cross sections for 2π annihilations.

		Forward π^-, $\cos\theta = 0.99$				Forward π^+, $\cos\theta = -0.99$			
P (GeV/c)	s (GeV^2)	t [(GeV/c)^2]	u [(GeV/c)^2]	$d\sigma/d\Omega$ (μb/sr)	$d\sigma/du$ [μb/(GeV/c)^2]	t [(GeV/c)^2]	u [(GeV/c)^2]	$d\sigma/d\Omega$ (μb/sr)	$d\sigma/du$ [μb/(GeV/c)^2]
0.700	3.957	−0.43	−1.72	156.3 ± 52.1	1510 ± 504	−1.72	−0.43	123.6 ± 31.9	1194 ± 308
0.870	4.161	−0.38	−1.98	70.7 ± 12.6	550 ± 98	−1.98	−0.38	96.9 ± 15.9	753 ± 124
0.990	4.320	−0.35	−2.17	54.1 ± 6.7	370 ± 46	−2.17	−0.35	97.9 ± 9.9	668 ± 67
1.120	4.502	−0.32	−2.38	31.5 ± 5.1	190 ± 31	−2.38	−0.32	87.4 ± 15.2	527 ± 92
1.340	4.830	−0.28	−2.75	31.6 ± 5.5	159 ± 28	−2.75	−0.28	27.8 ± 3.9	140 ± 20
1.450	5.001	−0.26	−2.94	34.3 ± 5.1	160 ± 24	−2.94	−0.26	25.0 ± 5.0	116 ± 23
1.590	5.225	−0.25	−3.18	19.1 ± 3.8	81 ± 16	−3.18	−0.25	15.7 ± 3.0	66 ± 12
1.710	5.420	−0.23	−3.39	18.2 ± 4.2	72 ± 17	−3.39	−0.23	16.7 ± 3.4	66 ± 13
1.815	5.594	−0.22	−3.57	17.4 ± 2.5	65 ± 9	−3.57	−0.22	9.1 ± 1.9	34 ± 7
2.000	5.906	−0.21	−3.90	19.2 ± 3.5	65 ± 12	−3.90	−0.21	3.9 ± 1.6	13 ± 5
2.160	6.179	−0.20	−4.18	17.6 ± 2.4	55 ± 7	−4.18	−0.20	5.4 ± 1.6	17 ± 5
2.400	6.596	−0.18	−4.61	9.9 ± 2.3	28 ± 7	−4.61	−0.18	2.8 ± 1.2	8 ± 3

TABLE VIII. Kaon extreme-angle differential cross sections for $2K$ annihilations.

		Forward K^-, $\cos\theta = 0.99$				Forward K^+, $\cos\theta = -0.99$			
P (GeV/c)	s (GeV^2)	t [(GeV/c)^2]	u [(GeV/c)^2]	$d\sigma/d\Omega$ (μb/sr)	$d\sigma/du$ [μb/(GeV/c)^2]	t [(GeV/c)^2]	u [(GeV/c)^2]	$d\sigma/d\Omega$ (μb/sr)	$d\sigma/du$ [μb/(GeV/c)^2]
0.700	3.957	−0.29	−1.42	10.9 ± 10.9	120 ± 120	−1.42	−0.29	63.0 ± 23.1	695 ± 254
0.870	4.161	−0.25	−1.66	19.5 ± 7.7	172 ± 68	−1.66	−0.25	16.3 ± 10.8	143 ± 95
0.990	4.320	−0.23	−1.84	14.6 ± 4.4	112 ± 34	−1.84	−0.23	33.9 ± 6.6	261 ± 51
1.120	4.502	−0.21	−2.05	12.0 ± 3.7	81 ± 25	−2.05	−0.21	23.6 ± 11.0	159 ± 75
1.340	4.830	−0.18	−2.40	7.1 ± 3.3	40 ± 19	−2.40	−0.18	13.5 ± 3.8	76 ± 21
1.450	5.001	−0.17	−2.58	12.7 ± 5.5	66 ± 28	−2.58	−0.17	4.1 ± 2.9	21 ± 15
1.590	5.225	−0.16	−2.82	12.0 ± 3.2	56 ± 15	−2.82	−0.16	4.0 ± 2.0	19 ± 9
1.710	5.420	−0.15	−3.02	7.7 ± 3.7	33 ± 16	−3.02	−0.15	0.0	0
1.815	5.594	−0.14	−3.20	8.8 ± 2.0	36 ± 8	−3.20	−0.14	1.2 ± 0.9	5 ± 4
2.000	5.906	−0.13	−3.53	10.2 ± 2.9	37 ± 11	−3.53	−0.13	0.6 ± 1.0	2 ± 4
2.160	6.179	−0.12	−3.81	7.4 ± 1.9	25 ± 6	−3.81	−0.12	1.1 ± 1.1	4 ± 4
2.400	6.596	−0.12	−4.23	6.5 ± 2.1	20 ± 6	−4.23	−0.12	0.0	0

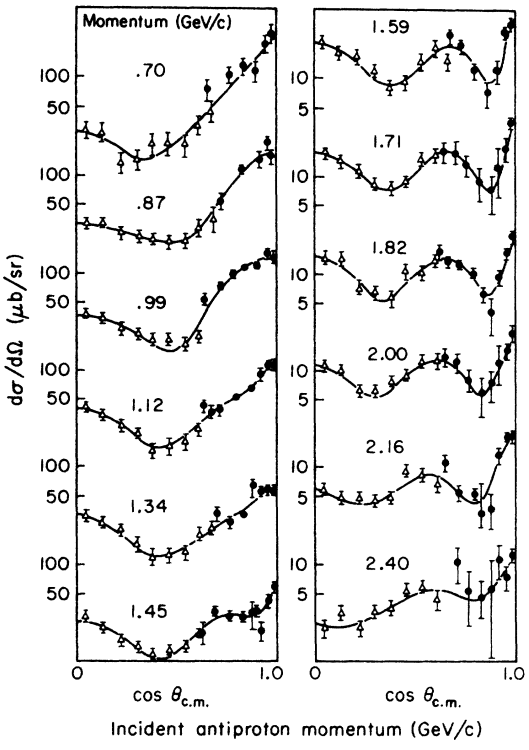

FIG. 6. Folded pion differential cross sections with Legendre-polynomial fit (solid curve). The solid circles are data from this experiment, and the open triangles are from Fong *et al.* (Ref. 2).

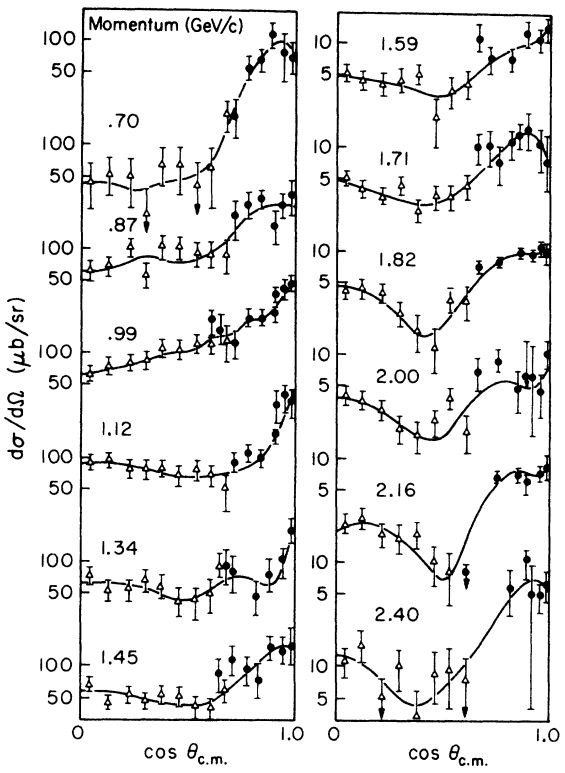

FIG. 7. Folded kaon differential cross sections with Legendre-polynomial fit (solid curve). The solid circles are data from this experiment and the open triangles are from Fong *et al.* (Ref. 2).

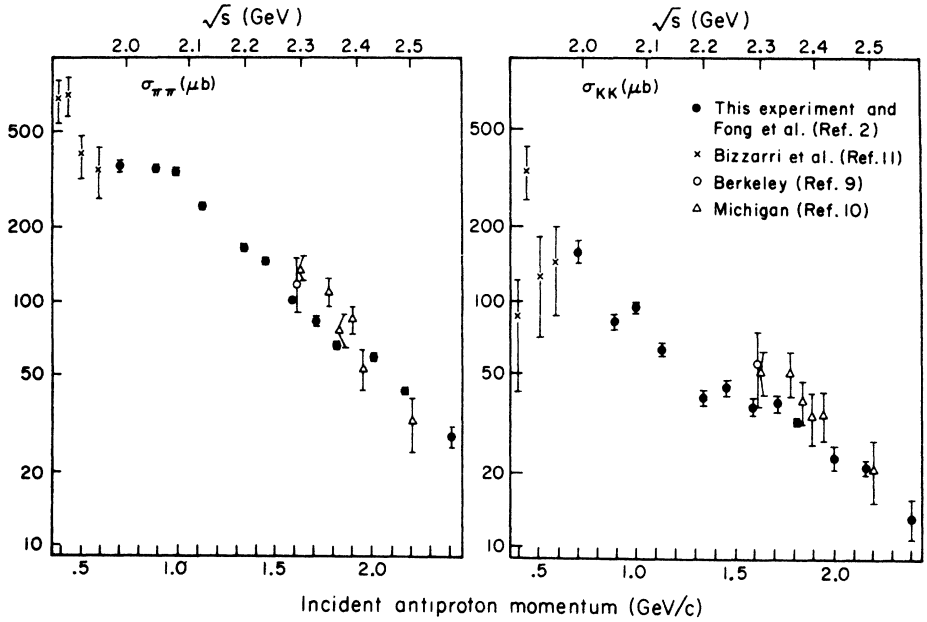

FIG. 8. Total annihilation cross sections for charged-pion pairs and charged-kaon pairs obtained from the leading Legendre-expansion coefficient for the folded pion and kaon cross sections.

1.0 GeV/c. However, the two-kaon channel does not develop the double-dipped angular distribution observed in the two-pion channel.

The solid curves through the data in Figs. 6 and 7 are the Legendre-polynomial fits. Total cross sections obtained from the leading coefficients for these fits are plotted for both the two-pion and two-kaon annihilation channels in Fig. 8. The most striking feature of the energy dependence of these total cross sections is the broad shoulder at 1.0 GeV/c ($s = 4.33$) in the two-pion annihilation channel. The over-all energy dependences of the total cross sections are $\sim s^{-6.3}$ and $s^{-4.6}$ for the two-pion and the two-kaon annihilations, respectively.

The most prominent features of the energy dependence of the remaining Legendre coefficients (Fig. 9) are the behavior of the a_6 and a_8 coefficients in the regions between 0.8 and 1.8 GeV/c for the two-pion annihilation. The peaking of the a_8 coefficient at 1.6 GeV/c combined with the fact that all other coefficients are relatively small at this momentum suggests that a P_4 Legendre polynomial or a combination of P_l^m associated Legendre polynomials simulating a P_4 Legendre polynomial dominates the amplitude at that momentum. Except for the fall and slight fluctuations of the a_2, a_4, and a_6 coefficients with increasing momentum from the low momenta (0.7–1.0 GeV/c), the Legendre coefficients of the two-kaon annihilation show no interesting structure.

Finally, it can be seen from Figs. 10–13 that between 0.7 and 1.34 GeV/c in both two-pion and two-kaon annihilations the positively charged particle has a higher probability of going forward, contrary to simple charge-following considerations. This might mean for $\bar{p}p \to \pi^+\pi^-$ that Δ exchange is the dominant mechanism. It is interesting to note that the relatively symmetric two-pion cross sections persist up to high energies.[12] Although there is structure in the cross sections for a charged pion going forward in a two-pion annihilation, the cross sections for a charged kaon going forward fall approximately exponentially, the cross section for the K^+ forward having the greater negative slope. The cross section $d\sigma/du$ has an s dependence given by s^{-10} for a positive kaon going forward and by $s^{-5.2}$ for a negative kaon going forward.

V. INTERPRETATION OF DATA

A. Resonance Fit to Two-Pion Annihilation

Figure 14, which shows the center-of-mass momentum squared times the total two-pion annihilation cross section as a function of momentum, shows a pronounced peaking at a center-of-mass energy of 2.1 GeV. This peak has motivated a simple Breit-Wigner resonance-model fit to the

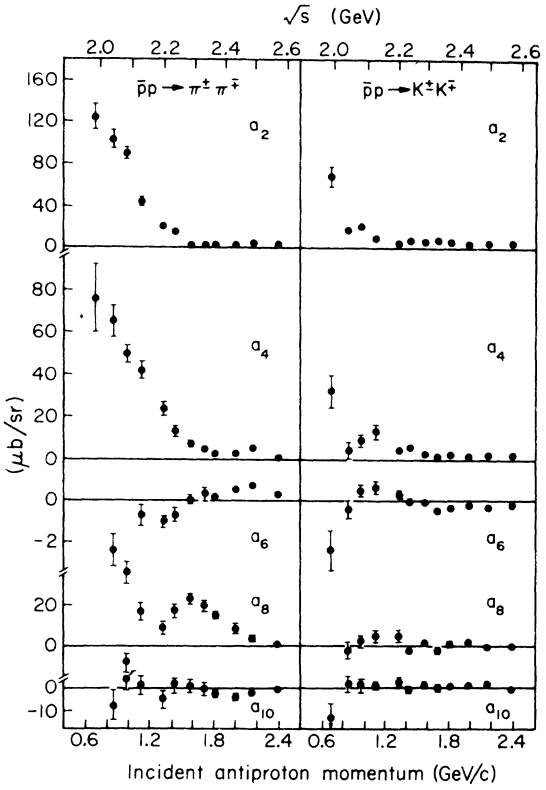

FIG. 9. Energy dependence of remaining Legendre-expansion coefficients to the folded pion and kaon cross sections.

two-pion annihilation data. A similar plot, Fig. 15, for the two-kaon annihilation data shows no such structure.

Because of the limited angular range of the data in which the sign of the charge of the forward-going particle could be determined, a resonance fit to the two-pion annihilation was made to the folded data only. This was considered reasonable since (a) the forward-backward asymmetry of the two-pion annihilation is $\lesssim 2.0$ (Fig. 10) over the entire range of incident antiproton momenta except near 2.0 GeV/c, and (b) energy-averaged bubble-chamber data between 1.6- and 2.2-GeV/c incident antiproton momenta are nearly symmetric.[22]

Blatt and Biedenharn[23] give an expression for the reaction-amplitude partial-wave decomposition of incident particle and target of arbitrary spins interacting to form two final-state particles of arbitrary spins. Their expression can be greatly simplified for the annihilation reactions studied in this experiment by the quantum-number considerations given below.[24]

Charge conjugation for a particle-antiparticle pair is given by the equation

$$C = (-1)^{l+s}, \tag{9}$$

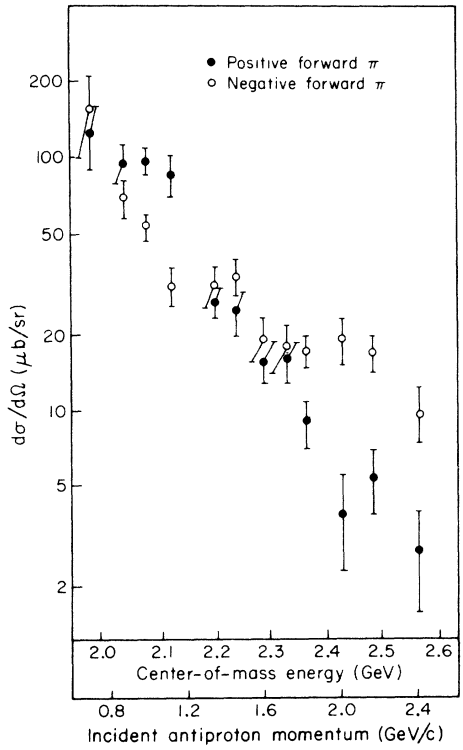

FIG. 10. Pion differential cross sections $d\sigma/d\Omega$ at $|\cos\theta| = 0.99$.

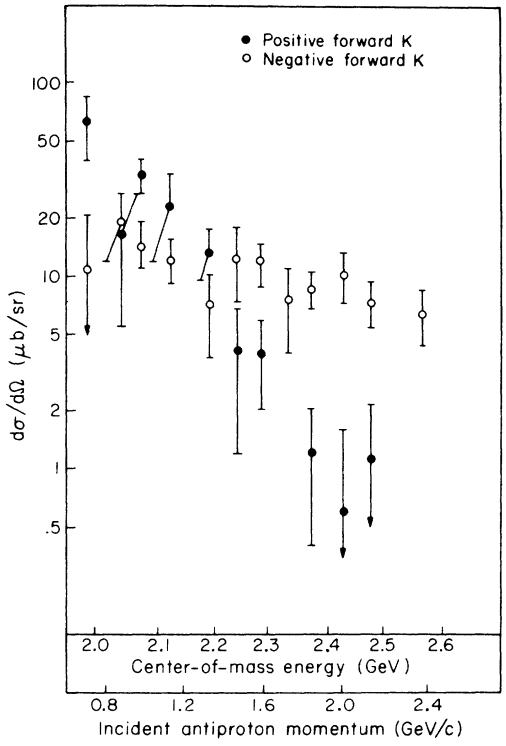

FIG. 11. Kaon differential cross sections $d\sigma/d\Omega$ at $|\cos\theta| = 0.99$.

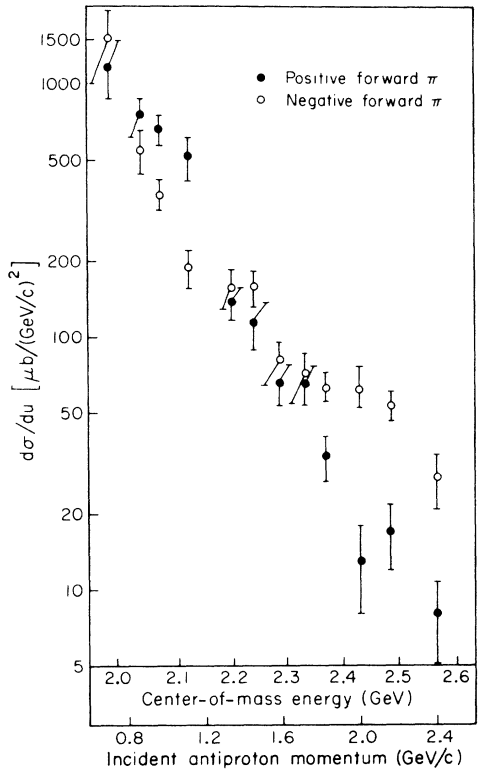

FIG. 12. Pion differential cross sections $d\sigma/du$ at $|\cos\theta| = 0.99$.

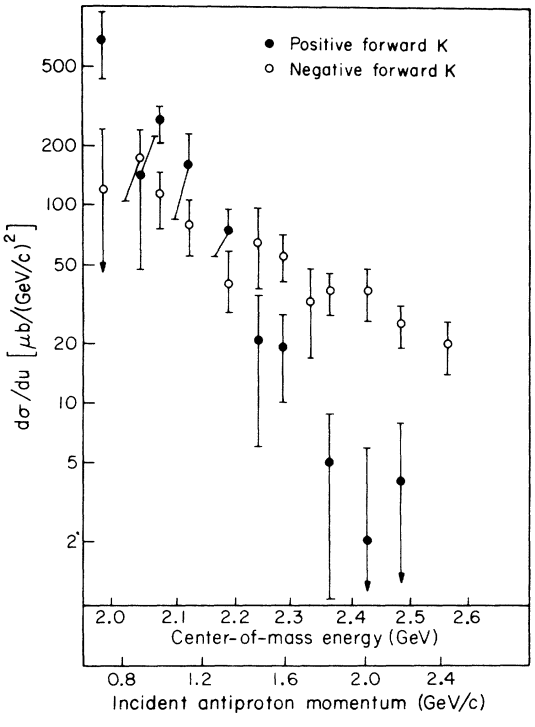

FIG. 13. Kaon differential cross sections $d\sigma/du$ at $|\cos\theta| = 0.99$.

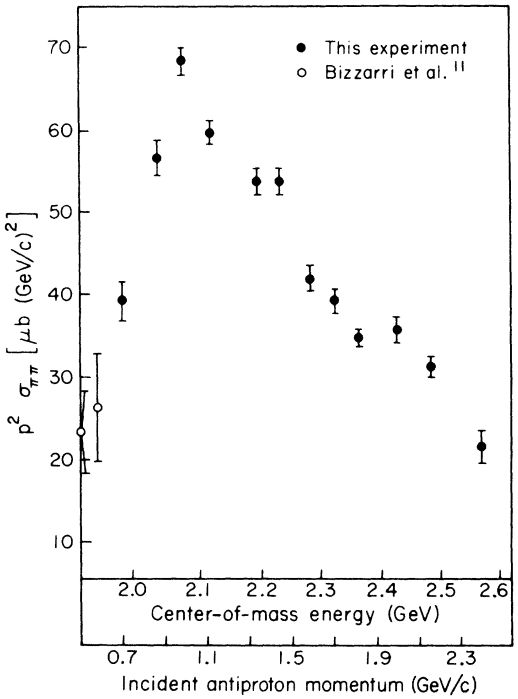

FIG. 14. Pion total cross sections multiplied by the center-of-mass incident antiproton momentum squared.

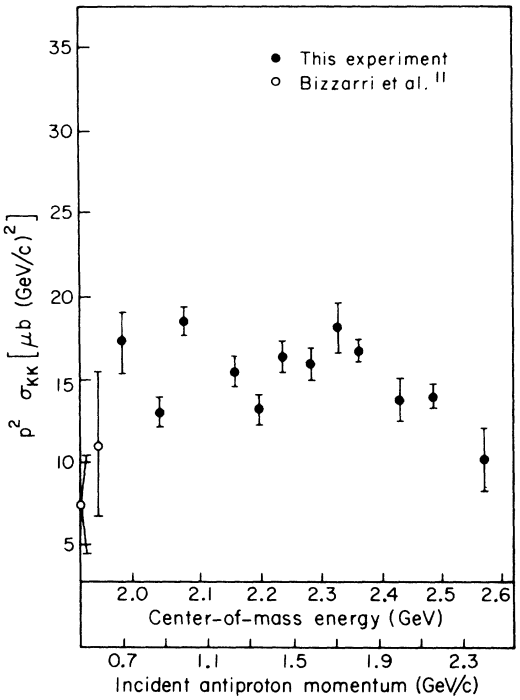

FIG. 15. Kaon total cross sections multiplied by the center-of-mass incident antiproton momentum squared.

while the parities of a boson-antiboson pair and a fermion-antifermion pair are given by

$$P_{\text{boson-antiboson}} = (-1)^l , \tag{10a}$$

$$P_{\text{fermion-antifermion}} = (-1)^{l+1} . \tag{10b}$$

Since the $\bar{p}p$ system comprises a fermion-antifermion pair, the $\pi^+\pi^-$ system is a boson-antiboson pair, and the total spin J of the pion-antipion system equals its orbital spin l since the pions have intrinsic spin s equal to zero, Eqs. (9) and (10) can be combined to give

$$J = l + 1 \ (\text{mod } 2) . \tag{11}$$

Furthermore, since the maximum intrinsic spin s available in the $\bar{p}p$ system is 1, Eq. (11) further simplifies to

$$J = l \pm 1 . \tag{12}$$

Assuming charge-conjugation conservation in the annihilation reactions and in the use of Eq. (9) yields

$$J = l + s . \tag{13}$$

Equations (12) and (13) then show that the $\bar{p}p$ system can annihilate into two pion pairs only if $s = 1$. Also note that the interchange of π^+ and π^- gives $(-1)^I$ for the isospin part and $(-1)^J$ for the spatial part, requiring I and J even, since pions are bosons.

Taking these quantum numbers and isotopic spin into account, the two-pion annihilation reaction cross section can be written

$$\frac{d\sigma}{d\Omega} = \frac{\pi}{2K^2}\left[\left(\left|\sum_{J=1}^{\infty}\left\{\left[\tfrac{1}{2}(J+1)\right]^{1/2}\left[\tfrac{1}{2}T_1^{J=l+1}+\left(\tfrac{1}{6}\right)^{1/2}T_0^{J=l+1}\right]-\left(\tfrac{1}{2}J\right)^{1/2}\left[\tfrac{1}{2}T_1^{J=l-1}+\left(\tfrac{1}{6}\right)^{1/2}T_0^{J=l-1}\right]\right\}Y_J^1(\theta,\phi)\right|\right)^2\right.$$
$$\left. + \frac{\pi}{4K^2}\left(\left|\sum_{J=0}^{\infty}\left\{\sqrt{J}\left[\tfrac{1}{2}T_1^{J=l+1}+\left(\tfrac{1}{6}\right)^{1/2}T_0^{J=l+1}\right]+(J+1)^{1/2}\left[\tfrac{1}{2}T_1^{J=l-1}+\left(\tfrac{1}{6}\right)^{1/2}T_0^{J=l-1}\right]\right\}Y_J^0(\theta,\phi)\right|\right)^2\right], \tag{14}$$

where the subscript on the T matrix is the isotopic spin and the superscript is the orbital angular momentum, k is the antiproton center-of-mass wave number, and the Y's are spherical harmonics. To obtain the expression for the folded cross section, the cross section obtained from Eq. (14) by the replacements $\theta \to \pi - \theta$ and $\phi \to \phi + \pi$ is added to the cross section calculated from Eq. (14).

The assumption of resonance-dominated amplitudes permits the substitution of a standard resonance (plus constant complex background terms) for the T matrix. Letting

$$T^{J=l+1} = \frac{A_J}{\epsilon_J - i} + A_J' , \tag{15a}$$

$$T^{J=l-1} = \frac{B_J}{\epsilon_J - i} + B_J' , \tag{15b}$$

where

$$\epsilon_J = -(s - m_{R_J}{}^2)/m_{R_J}\Gamma_J \tag{16}$$

is the total center-of-mass energy squared, m_{R_J} is the mass of the resonance, Γ_J is the full width of the resonance, and A_J and B_J are real numbers related to the partial production and decay widths in the two-meson annihilation channels, the expression for the folded cross section can be fitted to the folded data.[25]

The resonance-model expressions for the folded data have been fitted to the data of this experiment and the experiment of Fong *et al.*[26] by means of a nonlinear gradient fitting program using the method developed by Powell.[27] Resonance parameters for the best attempt to fit the folded cross sections, which included constant, complex background terms in the $J=1, 2, 3$ partial waves and allowed strengths, masses, and widths of the resonances as well as the background parameters to vary, are given in Table IX. (Neither the width nor the parameters A_J or B_J were energy-dependent in this fit.) As can be seen from Table IX, $J=3$ and $J=5$ were the dominant spins required to reproduce the folded data, due to the fact that the spherical harmonics Y_3^1 and Y_5^1 can interfere to give a term similar to $|Y_4^0|^2$ without the strong peaking near $|\cos\theta_{\text{c.m.}}|=1.0$, characteristic of this polynomial. The solid lines in Figs. 16–18 show how well this resonance-model fit reproduces the two-pion annihilation data.

Two resonances of spin $J=3$ and $J=5$ are theoretically predicted to exist in this energy region in a quark model for boson resonances described by Goldhaber and Goldhaber.[28] Their model predicts two heavy isospin-1, negative-parity meson resonances with total spin 3 and 5 at s values of ~4.3 and ~4.9, respectively, in reasonably good agreement with the resonance parameters obtained in the above fit.

Recently a Yale group has measured the asymmetry for annihilation of antiprotons or polarized protons at 1.6 GeV/c. Their data suggest that more even J contributions are necessary than are given by our model.[13]

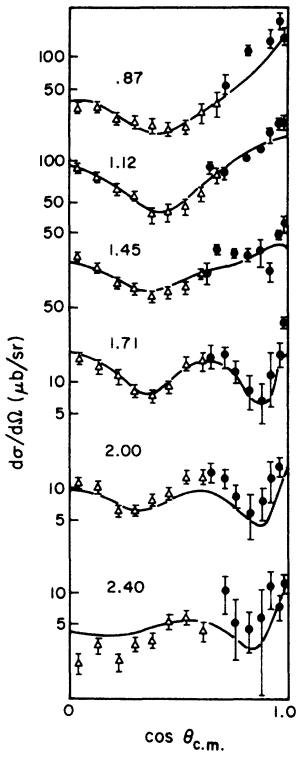

FIG. 16. Resonance fit to pion folded differential cross sections (solid curve).

TABLE IX. Fitted resonance parameters[a] for the folded $\bar{p}p \to \pi^+\pi^-$ data.

$A_1' = -0.062 - i0.015$

$B_1' = -0.041 - i0.011$

$A_2' = 0.019 + i0.00$

$B_2' = 0.023 + i0.00$

$A_3' = 0.022 + i0.091$

$B_3' = -0.024 + i0.128$

$A_3 = -0.426$, $B_3 = -0.093$, $M_3 = 2.132$ GeV,

$\Gamma_3 = 0.320$ GeV, $s = 4.52$ GeV^2

$A_5 = 0.048$, $B_5 = -0.065$, $M_5 = 2.287$ GeV,

$\Gamma_3 = 0.159$ GeV, $s = 5.24$ GeV^2

[a] Since these resonances decay into two pions and J = odd; $I=1$, $P=-$, and $G=+$ for both.

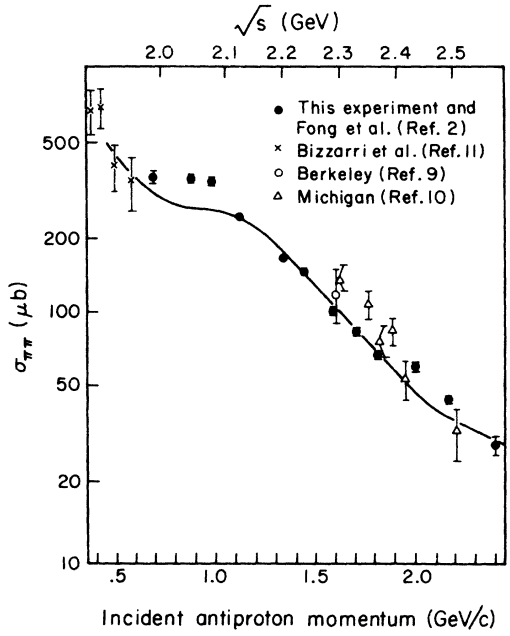

FIG. 17. Resonance fit to pion total cross sections (solid curve).

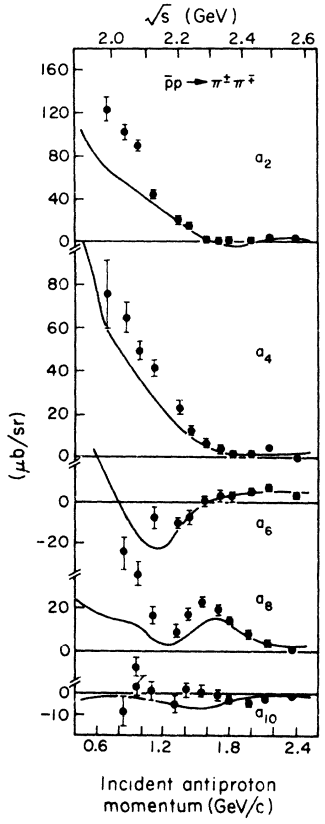

FIG. 18. Resonance fit to pion Legendre-expansion coefficients (solid curve).

B. Comparison of the Extreme-Angle Annihilation Data with πp and Kp Backward-Scattering Data Using Crossing Relations

Figure 2 shows how the u-channel exchange amplitudes for the annihilation reactions $\bar{p}p \to \pi^{\pm}\pi^{\mp}$ and $\bar{p}p \to K^{\pm}K^{\mp}$ are related to the backward elastic scattering reactions $\pi^{\pm}p \to p\pi^{\pm}$ and $K^{\pm}p \to pK^{\pm}$. In the limit of infinite energy Van Hove has shown by an extension of the Pomeranchuk theorem that the s-channel amplitude in elastic scattering becomes equal to the u-channel amplitude.[29] Assuming that the annihilation cross section $d\bar{\sigma}/du$ is dominated by the same u-channel exchanges as the backward-scattering cross section $d\sigma/du$, the relation between them is

$$\lim_{t\to\infty}\frac{d\bar{\sigma}}{du}(t,u)=\tfrac{1}{2}\lim_{s\to\infty}\frac{d\sigma}{du}(s,u). \tag{17}$$

The factor $\frac{1}{2}$ is the ratio of initial spin states for the meson-nucleon system to the antiproton-proton system.

At lower energies more detailed knowledge of the u-channel scattering amplitude is necessary before a crossing relation similar to Eq. (17) can be obtained. Within the framework of the Regge theory of fermion trajectory exchanges Barger and Cline[30] have derived the expression

$$\frac{d\bar{\sigma}}{du}=\frac{1}{2}\frac{d\sigma}{du}\frac{[s-(M+\mu)^2][s-(M-\mu)^2]}{s[s+u+2D^2]} \tag{18}$$

assuming that the invariant amplitude is an even function of $\sqrt{u}$ and is dominated by a single Regge exchange. Equation (18), in which M is the nucleon mass, μ is the meson mass, and $D^2=M^2-\mu^2$, reduces to Eq. (17) in the limit $s\to\infty$.

A comparison has been made between the extreme-angle annihilation data obtained in this experiment and πp and Kp backward elastic scattering data obtained in two earlier experiments using essentially the same experimental apparatus. This comparison, shown in Fig. 19, has been made at fixed $\cos\theta_{\text{c.m.}}=0.99$ instead of fixed u to increase the range of s in the comparison; u varies in value between -0.43 and -0.18 $(\text{GeV}/c)^2$ for the two-pion annihilation and between -0.29 and -0.12 $(\text{GeV}/c)^2$ for the two-kaon annihilation over the incident antiproton momentum range of this experiment. The backward-scattering cross sections shown in Fig. 19 have been multiplied by the kinematic crossing factor on the right-hand side of Eq. (18), and all errors are statistical.[31,7]

The comparison of the $\bar{p}p \to \pi^-\pi^+$ to $\pi^+p \to p\pi^+$ [reaction (1)] shows reasonable agreement everywhere except near $s=5.0$ GeV^2, where there is a strong dip in the backward π^+p cross section. Considering the many resonances and the large num-

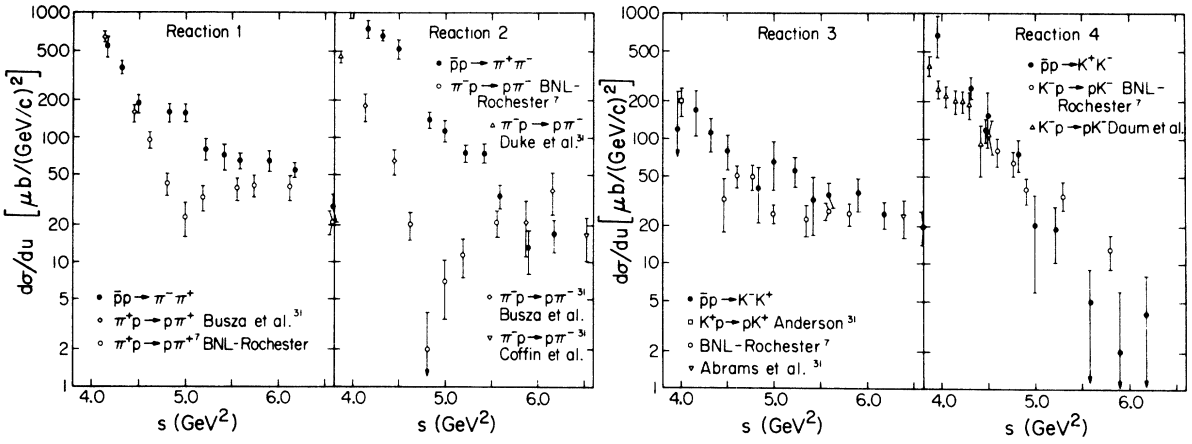

FIG. 19. Comparison of backward-scattering and annihilation reactions as a function of s at fixed $|\cos\theta_{c.m.}| = 0.99$ for the annihilation. The backward-scattering cross sections have been multiplied by the factor given in Eq. (18) in all cases. References for the backward-scattering cross sections are given in Refs. 7 and 28.

ber of possible exchanges, the comparison is somewhat better than might be expected. It is also interesting to note that both cross sections show similar shoulders at $s = 6.0$ GeV^2.

In the comparison of $\bar{p}p \to \pi^+\pi^-$ to $\pi^-p \to p\pi^-$ [reaction (2)], direct-channel effects, specifically the $N^*(2190)$, eliminate any quantitative agreement between them. Good agreement for these reactions would not be expected except at high momenta where the influence of the direct-channel resonances in πp scattering gives only small contributions to the complete scattering amplitude. At 5 GeV/c the agreement for reaction (1) is still better than for reaction (2) despite the fact that reaction (2) has only one exchange amplitude.

The agreement in the comparisons of $\bar{p}p \to K^-K^+$ to $K^+p \to pK^+$ [reaction (3)] and $\bar{p}p \to K^+K^-$ to $K^-p \to pK^-$ [reaction (4)] is striking, especially in view of the low momenta at which the comparison is being made. The agreement for reaction (3) is not surprising, since the backward K^+p scattering data can be fitted with an exchange-degenerate $\Lambda_\alpha, \Lambda_\gamma$ exchange which satisfies the requirements for Eq. (18) to be valid.[32] However, the good agreement for reaction (4) is not expected, since it is usually believed that K^-p backward scattering is dominated by direct-channel amplitudes.[33] The agreement for both pairs of reactions continues up to 5 GeV/c.[12]

At high momenta comparisons can be made between the above pairs of cross sections as a function of u for fixed s. The results of these comparisons are shown in Fig. 20, where the annihilation data have been averaged over four different momenta (ranging from $s = 5.4$ to $s = 6.2$ GeV^2) in order to improve the statistics, and the backward-scattering data have been multiplied by the crossing factor in Eq. (18) as before. For reaction (2) there is no significant disagreement over the range of u. Reactions (1) and (3), which show fair agreement near $\theta_{c.m.} = 180°$, differ markedly away from this point, possibly because the scattering amplitude is no longer even in the replacement of $\sqrt{u}$ by $-\sqrt{u}$ away from the center-of-mass angles. The K^-p backward-scattering cross sections [reaction (4)] do not agree quite as well as we had initially reported.[34]

VI. CONCLUSIONS

The two-pion annihilation data obtained in this experiment have been found to be consistent with the interpretation that the direct-channel (resonance) effects dominate the amplitude over the momentum region covered by this experiment. Evidence for these resonances has been obtained from the strong peaking in the total pion annihilation cross section near 1.0 GeV/c shown in Fig. 14, and the reasonable fit to the folded angular distributions obtained from a simple $J = 3$ and $J = 5$ two-resonance model shown in Figs. 16–18. Furthermore, the resonance parameters of the low-mass resonance (2.13 GeV) obtained in the resonance fit to the folded pion annihilation data are in reasonable agreement with the resonance parameters of the $B = 0$ structure observed by Anderson *et al.*[14] at a mass of 2.09 GeV. The stable parameters of this resonance with variations in numbers of resonances and backgrounds included in the fitting procedure are the mass 2.12 ± 0.05 GeV and the spin $J = 3$. Although the position of the upper-mass resonance (2.28 GeV) is sensitive to background contributions and varies between 2.2 and 2.5 GeV depending on the type of resonance model used, a

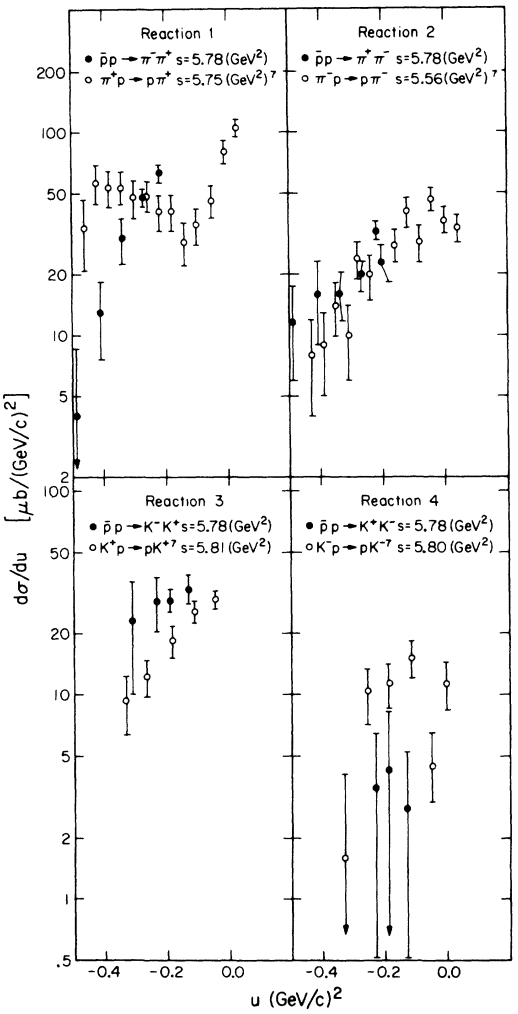

FIG. 20. Comparison of backward-scattering and annihilation reactions as a function of u at approximately the same value of s. The annihilation data have been averaged over four momenta with a mean s of 5.78 GeV^2, π^+p, π^-p, K^+p, and K^-p backward-scattering data are at 5.75, 5.56, 5.81, and 5.80 GeV^2, respectively. All backward-scattering cross sections are from Ref. 7.

large spin-5 contribution is needed in the amplitude to reproduce the folded data in the vicinity of 1.7 GeV/c, where available data have shown the complete unfolded distribution to be relatively symmetric about $\cos\theta_{c.m.} = 0$.

The complexity of the pion-annihilation scattering amplitude containing up to six partial waves ($J < 6$) has made it impossible to establish the uniqueness of the fitting parameters. More complete data will be needed before the annihilation amplitudes can be uniquely determined.

A possible reason for the failure of this experiment to detect more of the previously reported $B = 0$ structures[35] in the mass range of this experiment is due to the lack of sufficient mass resolution to detect the narrow structures. It is unlikely that a resonance with width less than 40 MeV and producing a resonance cross section less than half the measured cross section would be observed in these results.

Another possible explanation for the failure of this experiment to detect some of the reported $B = 0$ structures may be related to an angular momentum barrier for the $\bar{p}p$ system. The maximum total spin which can be formed in the $\bar{p}p$ system, assuming a proton interaction radius of ~1.0 F, is smaller than the total spin required to couple to the CERN R, S, T, and U structures.[36]

The two-kaon annihilation data obtained in this experiment have been found to be consistent with the interpretation that exchange effects dominate the amplitude over the momentum region of the experiment. Although the two-kaon folded differential cross sections have been fitted with the two-pion resonances and an additional spin-4 resonance with variable parameters, the simplicity of the folded angular distributions would not seem to warrant such complexity *a priori*. (A resonance with negative G parity would not couple to the two-pion annihilation channel.) There is no evidence of direct-channel structure either in the total two-kaon annihilation cross sections (Fig. 15) or the extreme-angle differential cross sections (Fig. 11). Furthermore, reasonable agreement has been obtained between the extreme-angle two-kaon annihilation data and the Kp backward-scattering data, assuming that the amplitudes are dominated by u-channel exchanges.

If the amplitudes of the reactions $K^-p \to pK^-$ and $\bar{p}p \to K^+K^-$ are dominated by an exchange, the exchanged particle or trajectory must be exotic (mesons which cannot be formed from a quark-antiquark pair). Presently available experimental information does not exclude the possibility of a Reggeized $Z^{*++}(S=1, B=1)$ exchange with $\alpha(0) \approx -4.0 \pm 1.0$.[37] If such a trajectory had a slope of 1 (GeV/c)$^{-2}$, it would pass through the vicinity of the higher $I=1$ peaks of the K^+p total cross section.[38]

The continued poor agreement of the reactions $\pi^-p \to p\pi^-$ and $\bar{p}p \to \pi^+\pi^-$ up to 5 GeV/c despite the supposed presence of a single dominant exchange amplitude would suggest that the crossing relations are probably governed by some mechanism other than Regge-exchange amplitude.

ACKNOWLEDGMENTS

We are indebted to many people for their contributions, assistance, and encouragement during the course of this experiment. In particular, we

thank the members of the AGS operating and planning staff, of the Brookhaven Central Scientific Computing Facility, of the Cryogenics Group, and of the Instrumentation Division. We also thank Dr. J. Fischer for designing and constructing the spark chambers; W. Friedler, H. Grau, J. Gatz, and J. Sanders for technical assistance; Dr. C. C. Shih, of Brookhaven National Laboratory, and Dr. S. Tewksbury, formerly at the University of Rochester, for helpful discussions and suggestions regarding the application of crossing relations; and Dr. R. L. Cool for advice and support in this work. One of us (H.N.) would also like to thank members of the Research Computing Center at the University of Massachusetts for assistance and financial support.

---

*Work performed under the auspices of the U. S. Atomic Energy Commission. Prepared under Contract No. AT(11-1)-68 for the San Francisco Operations office, U. S. Atomic Energy Commission.

† Present address: Physics Department, Mount Holyoke College, South Hadley, Mass.

‡ Present address: CERN, Geneva, Switzerland.

§ Present address: University of Madagascar, Tananarive, Malagasy Republic.

¶ Present address: California Institute of Technology, Pasadena, California.

[1]"Folded" is used here to mean the summed cross sections $d\sigma/d\Omega(\theta) + d\sigma/d\Omega(\pi-\theta)$.

[2]D. Fong, Ph.D. thesis, Caltech, 1968 (unpublished); J. K. Yoh *et al.*, Phys. Rev. Letters 23, 9 (1969).

[3]R. J. Abrams *et al.*, Phys. Rev. Letters 18, 1209 (1967).

[4]E. W. Anderson *et al.*, Phys. Rev. Letters 22, 1390 (1969).

[5]M. N. Focacci *et al.*, Phys. Rev. Letters 17, 890 (1966).

[6]B. Y. Oh *et al.*, Phys. Rev. Letters 24, 1257 (1970).

[7]K^-p: A. S. Carroll *et al.*, Phys. Rev. Letters 23, 887 (1969); C. A. Smith, Ph.D. thesis, University of Rochester, 1970 (unpublished). K^+p: A. S. Carroll *et al.*, Phys. Rev. Letters 21, 1282 (1969); S. K. Tewksbury, Ph.D. thesis, University of Rochester, 1969 (unpublished). $\pi^\pm p$: A. S. Carroll *et al.*, Phys. Rev. Letters 20, 607 (1968).

[8]See, for example, V. Barger and D. Cline, Phys. Letters 25B, 415 (1967).

[9]G. R. Lynch *et al.*, Phys. Rev. 131, 1287 (1963).

[10]J. W. Chapman *et al.*, Phys. Rev. Letters 21, 1718 (1968).

[11]R. Bizzarri *et al.*, Istituto di Fisica dell'Universita di Roma Nota Interna No. 213, 1969 (unpublished).

[12]C. Baglin *et al.*, in *Proceedings of the Amsterdam International Conference on Elementary Particles, 1971*, edited by A. G. Tenner and M. Veltman (North-Holland, Amsterdam, 1972).

[13]A. Etlein *et al.*, Bull. Am. Phys. Soc. 16, 137 (1971).

[14]B. A Leontic and J. Teiger, BNL Report No. 50031 (T447) (unpublished). We thank B. A. Leontic and his collaborators for permission to use this counter.

[15]J. K. Yoh, Ph.D. thesis, Caltech, 1970 (unpublished).

[16]See Ref. 7.

[17]S. K. Tewksbury, Ph.D. thesis, University of Rochester, 1969 (unpublished).

[18]The wire spark chambers were constructed by J. Fischer of the Instrumentation Division of BNL. See J. Fischer, BNL Report No. 11031 (unpublished).

[19]Similar to the type described by V. Perez-Mendez and J. M. Pfab [Nucl. Instrum. Methods 33, 141 (1965)].

[20]The vertex and copunctuality were determined by minimizing the equation

$$\text{Copunctuality} = \left[\tfrac{1}{3}\sum_{i=1}^{3}(\vec{x}^i + \vec{e}^i t_1 - \vec{a})^2\right]^{1/2},$$

where $\vec{x}^i$ is the $z=0$ intercept of track i, $\vec{e}^i$ is the unit vector of track i, t_1 is the track length to the point of closest approach, and $\vec{a}$ is the position vector of the vertex for the three tracks.

[21]See Ref. 10.

[22]See Ref. 10.

[23]J. M. Blatt and L. C. Biedenharn, Rev. Mod. Phys. 24, 258 (1952).

[24]The constraints on quantum numbers are discussed by D. B. Lichtenberg [*Meson and Baryon Spectroscopy* (Springer, New York, 1965)].

[25]Similar expression for the resonance amplitudes are used by V. D. Barger and D. B. Cline [Phys. Rev. 155, 1792 (1967)]. For details see W. Layson, Nuovo Cimento 27, 724 (1963); J. D. Jackson, *ibid.* 34, 1644 (1964).

[26]See Ref. 2.

[27]M. J. D. Powell, Computer J. 4, 303 (1965).

[28]G. Goldhaber and S. Goldhaber, in *Advances in Particle Physics*, edited by R. L. Cool and R. E. Marshak (Interscience, New York, 1968).

[29]L. Van Hove, Phys. Letters 5, 252 (1963).

[30]See Ref. 8.

[31]G. S. Abrams *et al.*, Phys. Rev. Letters 21, 1407 (1968); Particle Data Group, LBL Report No. UCRL-8030, 1970 (unpublished) and No. LBL-58, 1972 (unpublished); W. Busza *et al.*, Phys. Rev. 180, 1339 (1969); C. T. Coffin *et al.*, *ibid.* 159, 1169 (1967); C. Daum *et al.*, Nucl. Phys. B6, 273 (1968); P. J. Duke *et al.*, Phys. Rev. 166, 1448 (1968).

[32]See Ref. 14.

[33]Duality arguments may explain this agreement. See R. Dolen, D. Horn, and C. Schmid, Phys. Rev. 166, 1777 (1968).

[34]B. C. Barish *et al.*, Phys. Rev. Letters 23, 607 (1969).

[35]See Refs. 3–6.

[36]See Ref. 5.

[37]A Regge cut gives neither the correct energy dependence nor the magnitude. See V. Barger, C. Michael, and R. J. N. Phillips, Phys. Rev. 185, 1952 (1969).

[38]R. J. Abrams *et al.*, Phys. Rev. Letters 19, 259 (1967).